PNAS Nexus, 2024, 3, pgae237
https://doi.org/10.1093/pnasnexus/pgae237
Advance access publication 26 June 2024
Research Report

Understanding underlying physical mechanism reveals early warning indicators and key elements for adaptive infections disease networks

Linqi Wang[a,b], Kun Zhang[b], Li Xu[b] and Jin Wang[c,*]

[a]Center of Theoretical Physics, College of Physics, Jilin University, Changchun, Jilin, 130012, China
[b]State Key Laboratory of Electroanalytical Chemistry, Changchun Institute of Applied Chemistry, Chinese Academy of Sciences, Changchun, Jilin, 130022, China
[c]Department of Chemistry, Physics and Astronomy, State University of New York at Stony Brook, Stony Brook, NY 11794, USA
*To whom correspondence should be addressed: Email: jin.wang.1@stonybrook.edu
Edited By: Rui Reis

Abstract

The study of infectious diseases holds significant scientific and societal importance, yet current research on the mechanisms of disease emergence and prediction methods still face challenging issues. This research uses the landscape and flux theoretical framework to reveal the non-equilibrium dynamics of adaptive infectious diseases and uncover its underlying physical mechanism. This allows the quantification of dynamics, characterizing the system with two basins of attraction determined by gradient and rotational flux forces. Quantification of entropy production rates provides insights into the system deviating from equilibrium and associated dissipative costs. The study identifies early warning indicators for the critical transition, emphasizing the advantage of observing time irreversibility from time series over theoretical entropy production and flux. The presence of rotational flux leads to an irreversible pathway between disease states. Through global sensitivity analysis, we identified the key factors influencing infectious diseases. In summary, this research offers valuable insights into infectious disease dynamics and presents a practical approach for predicting the onset of critical transition, addressing existing research gaps.

Keywords: infectious disease, early warning signals, landscape, flux

Significance Statement

Understanding the mechanism of infectious diseases is crucial for human health, yet challenging. We revealed the underlying physical mechanism of adaptive infectious diseases using landscape and flux theory, providing a dynamical and thermodynamic origin for epidemic emergence. We proposed a predictive method based on average flux, entropy production rate and time irreversibility. Our study also demonstrated that early warning signals from time irreversibility often precede the conventional critical slowing down and flickering frequency, and can be extracted directly from the observable time series analysis, providing practical predictions. We further revealed key elements influencing adaptive infectious diseases from global sensitive analyses of barrier height, crucial for the understanding and control of diseases transmission.

Introduction

In recent years, there is a pressing need for in-depth research on the outbreak of infectious diseases and their transmission mechanisms within human communities, which has become a crucial topic in the scientific community (1–5). People have carried out significant studies on virus transmission and developed mathematical models of virus transmission (6–8). Based on the complex network theory, several a few virus propagation models in networks have been proposed (9–12). Mathematical models have played an important role in understanding the virus propagation and its impact on disease control (13). These models simulate the interconnectedness of individuals within a network structure, helping to reveal how diseases rapidly propagate in populations (14–17). Utilizing complex network theory, a powerful tool for simulating various behaviors as computer viruses and human infectious diseases (16, 18, 19), nodes in the network represent individuals or systems, while edges denote the connections between them. Studying the network's topology, patterns of node connections, and the mechanisms of information propagation provides insights into the dynamic spread of viruses or diseases within the network (20, 21). These approaches not only enable the simulation of the paths and speed of disease transmission but also

Competing Interest: The authors declare no competing interest.
Received: February 1, 2024. **Accepted:** June 3, 2024

facilitate the assessment of the effectiveness of different prevention and control strategies within the network. Through simulations on complex networks, one can comprehensively understand and predict patterns of disease spread, offering essential scientific foundations for devising effective countermeasures (22–25).

In the study of infectious disease, it is imperative to review the developmental history of infectious disease models, which have played a pivotal role in our understanding of the dynamics of disease transmission. Tracing back to 1,766, the first treatise exploring the dynamic models of epidemics was authored in the pursuit of understanding the spread of smallpox (26). By the early 20th century, mathematical models addressing the dynamic transmission of malaria were introduced (27). Subsequently, classical models as the Susceptible-Infectious-Recovered model proposed by Kermack and McKendrick (28) and complex network models emerged (20, 29). In recent decades, various epidemic models have been developed based on the Kermack-McKendrick model, including Susceptible-Infectious-Susceptible models, Susceptible-Infectious-Recovered model (30), and Susceptible-Exposed-Infectious-Recovered models with or without time delays (31, 32).

In the field of mathematical modeling of infectious diseases, there are generally several approaches: statistical models, deterministic models (33, 34), stochastic models (35, 36), and network models (9, 37, 38), among others. Statistical models are commonly employed in epidemiological and public health research, but they require a large amount of data samples (39). Deterministic models, on the other hand, utilize forms such as differential equations and difference equations. They assume that the sizes of susceptible and infected populations are continuous functions of time, describing the dynamic relationship between the rates of change and population size. Compared to statistical models, these models are less dependent on data and are suitable for prediction (40). People can directly benefit from the theory of dynamical systems and well-developed, readily available numerical methods. However, a disadvantage is that the structural constraints of these models often prevent them from accurately reflecting the infectivity profiles present in real-life scenarios (41). Stochastic models regard disease transmission as a random process and are typically applicable for managing small-scale populations, such as small communities or individual hospitals, or scenarios where infected individuals are highly active with numerous contacts (42, 43). However, due to the lack of mathematical tools, the mathematical analysis of stochastic models is more challenging, and model analysis relies mainly on extensive observations through numerical simulations. Network models can capture the complexity of human contact interactions, but they are typically static and may not accurately predict the dynamics of disease in dynamic networks (44). Deterministic epidemic models are mathematical models that describe the spread of epidemics through differential equations. Among them, the compartmental approach is a commonly used modeling technique, which divides the population into different compartments (or groups or states) and describes the transitions between them. These compartments represent different health or infection states in the population, such as susceptible individuals, infected individuals, and recovered individuals. Common compartmental models include the Susceptible-Infected-Susceptible (SIS) model, Susceptible-Infected-Recovered (SIR) model, Susceptible-Infected-Recovered-Susceptible (SIRS) model, etc. These models can be adjusted and expanded based on specific epidemiological characteristics and transmission mechanisms to better adapt to different epidemic situations and research needs. The SIS, SIR, and subsequent SIRS models categorize the host population into different infection classes. These classes interact with each other, and the actual spread of the virus in the population is carried out not linearly forward but with feedback, and this forms a network-like structure, also known as a transition diagram (39).

Compartmental models provide a theoretical framework for studying the spread of viruses or diseases, significantly enhancing our understanding of dynamic disease transmission in populations. These models serve as pivotal starting points in the field of infectious disease modeling, laying the foundation for subsequent research (30–32, 45, 46). In the SIS disease transmission model, individuals can only exist in two states: susceptible (S) and infected (I). A susceptible individual can become infected by an infected individual, recover from the infection, and return to the susceptible state, making them susceptible to reinfection. The SIR model introduces an additional state: recovered (R). Susceptible individuals can be infected by infected individuals, switching to the infected state. However, infected individuals can recover from the infection and become immune individuals, no longer susceptible to reinfection. The SIRS model builds upon the SIR model by incorporating the possibility of recovered individuals losing their immunity and becoming susceptible again. These renowned models have significantly aided in understanding disease transmission by depicting the transitions between susceptible, infected, and recovered individuals and their interactions. Despite their simplicity, they have demonstrated the capability to forecast outbreaks of childhood diseases (47).

While the classification and interactions among these model individuals reveal the complex dynamics of disease transmission, they often do not take into account the self-isolation of the host itself, and the self-protective behavior of the individual can significantly reduce the spread of disease, for example, in past Ebola Virus Disease (EVD) epidemics, behavior change has been the primary method to bring epidemics under control (48), in areas where Acquired Immune Deficiency Syndrome (AIDS) is endemic, the demand for condoms rises (49). Measles outbreaks are linked to the demand for rubella vaccines (50), the impact of individual precautions on epidemic transmission (51). When dealing with the constantly changing relational dynamics within real networks, this point becomes particularly evident. The local dynamics of the nodes within the network play a crucial role in influencing the changes in the network topology (52, 53). The complex interplay between the topology of adaptive networks and dynamical nodes may generate intricate global behaviors under simple local rules, a behavior already evident in various fields such as biology, genomics, and game theory (54). Recent research has made significant strides in investigating how people influence the spread of infectious diseases by studying link disruptions and rewiring (45). The incorporation of adaptive rewiring into network models has been demonstrated to facilitate the development of epidemiological models that accurately capture real-world scenarios, such as the coexistence of endemic and disease-free bistable states (46). Consequently, this augments our comprehension of the role of network rewiring in epidemic simulations, thereby furnishing valuable insights to inform more efficacious prevention and control strategies, for instance, in practice, individuals should take corresponding measures (55) to avoid contact with infected individuals to curb the occurrence of epidemics.

Despite significant advancements in infectious disease modeling (45, 46, 56), there are still challenges in theoretical predictions and the understanding of the physical mechanisms underlying infectious diseases. In recent years, emerging landscape and flux theory has been considered a promising approach to overcome

these challenges. Traditional infectious disease modeling primarily focuses on individual-level elements such as infection rates and immune status (13, 57). In contrast, landscape and flux theory places greater emphasis on the global perspective and underlying physical mechanisms (58–60). This shift towards a more global perspective is seen as a potential solution to the limitations faced by traditional models. The landscape and flux theory offers a holistic approach that considers the global dynamics of infectious diseases by incorporating insights from both the landscape and the fundamental physical processes at the lower levels. This paradigm shift holds the promise of providing a more comprehensive understanding of infectious disease dynamics and improving the accuracy of theoretical predictions.

In this study, we will reveal the dynamics and thermodynamic origins of saddle-node bifurcations (phase transitions) in infectious diseases based on an adaptive infectious disease network (46) from the perspective of non-equilibrium landscapes and flux theory (58, 59). We plan to reveal the role of potential landscapes as a global Lyapunov function, aiming for a more accurate quantification of the overall stability of the network system. Specifically, our focus will be on the dynamics and thermodynamic characteristics of infectious disease systems undergoing saddle-node bifurcations between endemic and disease-free states. We will employ the analysis of average flux, entropy production rate, and time irreversibility quantified by the differences in the cross-correlations of system states in the forward and backward time to effectively characterize and predict the occurrence and disappearance of endemic and disease-free states. This aspect has been relatively neglected in previous studies of adaptive network epidemiology (45, 46).

Additionally, we use the concept of flickering frequency (61) introduced before as an additional dynamic feature to enhance the comprehensive prediction of saddle-node bifurcations. Studies have indicated that flickering frequency may undergo changes as the system approaches to a critical point, potentially serving as an early indicator. By observing changes in flickering frequency, we can further anticipate critical transitions that the system might undergo, providing more ample time for preventive measures. Meanwhile, we will explore critical slowing down and time irreversibility, both serving as effective predictive indicators. They can together cooperate with flickering frequency offer a more comprehensive and reliable predictive framework. By integrating these dynamic and thermodynamic features, our aim is to provide a deeper insight into the dynamic mechanisms underlying the emergence of infectious diseases, enhancing the understanding of the dynamics of infectious disease transmission. Furthermore, this research contributes more comprehensively to the fields of study and applications related to public health and epidemiology.

Adaptive network SIRS infectious disease model

The network models of epidemics aim to simulate the spread of diseases in the real world, and their development relies on advancements in mathematics and physics (56). Moreover, because these models can be tested based on real data, they provide crucial feedback on physical principles. For a more realistic epidemic model, it is imperative to consider how individuals and populations adjust their behavior as they acquire more information. For example, during the COVID-19 pandemic, with the rapid dissemination of disease threat information through media, government policies, and interpersonal interactions, people have taken measures such as reducing contact with infected individuals or getting vaccinated to mitigate the risk of infection (55).

Recent studies have been focused on the interplay between dynamic social networks and the spread of infectious diseases. The adaptive network model considers the dynamic adjustment of network structure during disease transmission (45). Attention has turned to how interpersonal interactions influence the restructuring of connections within the populations. This network restructuring is seen as a socially driven response to disease spread, which in turn influences disease dynamics. Such modeling has led to the emergence of new dynamic instabilities and multiple attractor states. Gross et al. studied the SIS model with adaptive networks (45), where rewiring potentially leads to sustained transmission and a disease-free bistable state. Leah B. Shaw and Ira B. Schwartz generalized the SIS model of adaptive networks to the SIRS model of adaptive networks (46).

The mean-field methodology to describe the SIRS adaptive infectious disease network nodes and links in terms of probabilities, leads a set of mutually coupled ordinary differential equations (46). As shown in Fig. 1A, consider the spread of an infectious disease along a network with N nodes, K links, and connections among the nodes that do not allow multilinking or self-connecting. The nodes evolve according to the SIRS pattern, as shown in Fig. 1B. Considering that real-world network topologies can dynamically adjust according to the dynamic state of nodes, for example, humans tend to avoid being infected by avoiding contact with infected people. The links in this adaptive model dynamically rewire according to the infection status of the nodes to adapt to the spread of infection, and this rewiring can have a strong impact on the dynamics of the disease, thus tending to suppress the outbreak (56). Specifically, as illustrated in Fig. 1C, when there is contact between non-infected and infected individuals in the network, social pressure (to avoid infection) drives the

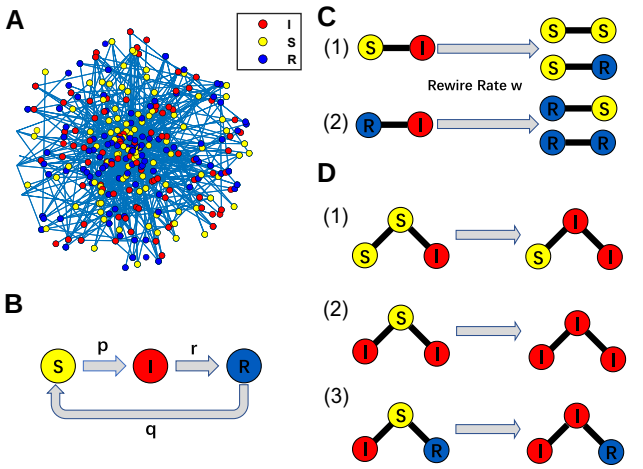

Fig. 1. A) Schematic diagram of simulated infectious disease transmission. There are three types of nodes in the whole network, which represent susceptible persons(S), infected persons(I), and recovered persons(R). B) Epidemic dynamics under the SIRS model. Susceptible individual S can be infected by infected individual I at rate p to become infected individual I, infected individual I can recover as immune recovered individual R at rate r, and recovered individual R may also lose immunity and re-become susceptible individual S at rate q. C) Adaptive network dynamics. During disease transmission, when a non-infected individual(S or R) comes into contact with an infected individual (SI link or RI link), the non-infected individuals S and R perform adaptive disconnection and rewiring (rewiring to the non-infected node S or R) at the rate w. (D) Three point term. Three-point links affect the evolution of links in the network.

Table 1. The variables in the mean-field equation.

Symbol	Interpretation
P_S	The probability of a node to be in state susceptible
P_I	The probability of a node to be in state infected
P_R	The probability of a node to be in state recovered
P_{II}	The probability that a randomly selected link connects a node in state infected to a node in state infected
P_{IS}	The probability that a randomly selected link connects a node in state infected to a node in state susceptible
P_{IR}	The probability that a randomly selected link connects a node in state infected to a node in state recovered
P_{SS}	The probability that a randomly selected link connects a node in state susceptible to a node in state susceptible
P_{SR}	The probability that a randomly selected link connects a node in state susceptible to a node in state recovered
P_{RR}	The probability that a randomly selected link connects a node in state recovered to a node in state recovered

Table 2. The parameters and values.

Symbol	Interpretation	Value
q	The resusceptibility rate	6.4×10^{-3}
K	Number of links	1×10^5
N	Number of nodes	1×10^4
r	The recovery rate for an infected node	2×10^{-3}
w	rewiring rate	4×10^{-2}
p	The infection rate	

dynamic rewiring of connections between nodes. This rewiring results from individuals adjusting their contact patterns to prevent the spread of disease. Therefore, the network, by changing the connection pattern, rewires nodes originally linked to infected individuals to other susceptible nodes, thus slows down the spread of infection. This process leads to a continuous evolution of the network structure, significantly influencing the mechanism of epidemic transmission. In addition, the model also takes into account the influence of three-point links in the network on the link evolution shown in Fig. 1D.

In this model, the dynamic state and topological structure of the network can both be described using mean-field quantities. In this network, only the probabilities of each node's state and the probabilities of all links are considered without taking into account the evolution of all nodes. The probability of each node being in a certain state in the network is influenced by the spreading dynamics of SIRS (Fig. 1B) and the rewiring dynamics (Fig. 1C). Specifically, in this SIRS propagation model, nodes can be in states of susceptible people (S), infected people (I), or recovered people (R), and any links or nodes that can affect the node's state or the network's connectivity during propagation or transmission can influence the node's current state. The temporal evolution of node states follows Eqs. 1–3, and the temporal evolution of links complies with Eqs. 4–Eqs. 9. Here, P_i represents the probability of a node being in state i, and P_{ij} represents the probability that a randomly selected link will connect states i and j. On the one hand, to account for the mutual influence between nodes and links, and on the other hand, for the sake of closure in the system, the model employs a moment closure approximation method for treating three-node motifs P_{ikj} ($P_{ikj} \approx P_{ik}P_{kj}/P_k$) (19, 62). Specifically, the probability of a three-node motif P_{ikj} is approximated as the product of the probability of ik links P_{ik} and the probability that a given node k has kj links P_{kj}/P_k, where i, j, and k can be susceptible (S), recovered (R), or infected (I). In Table 1, we give a specific explanation of each variable in the mean-field equation. Table 2 provides explanations and specific values for other parameters in the equations which are sourced from research paper (46).

One can combine the SIRS spreading dynamics with the rewiring dynamics to get the mean-field equations and provide a specific explanation for each term in the equations. Specifically speaking, the dynamics and topology of the adaptive network can be quantified using mean-field measures, such as the density of S-type nodes or the occurrence probability of SI links within the network, which are described in terms of probabilities. In an SIRS network, nodes are classified into three types: susceptible (S), infectious (I), and recovered (R), while links can be categorized into different types: SS, SI, SR, II, IR, and RR. As the epidemic progresses, these various types of nodes and links undergo evolution within the network, which is governed by a set of differential equations. The density or probability of any particular node or link within the network changes dynamically due to the SIRS propagation mechanism and rewiring dynamics.

In the evolution equation for node S, on average, its density or probability in the network is only influenced by nodes in the R state and SI links. This is because the recovery node R reverts to susceptible node S at a rate of q, leading to an increase in the probability or density of susceptibility. Meanwhile, the impact of SI links on node S is that susceptible node S gets infected along SI links at a rate of p, transforming into infectious node I, thereby reducing the probability of susceptibility for node S.

In the evolution equation for node I, on average, only SI-type links and nodes of type I will affect the evolution of node I. This is because susceptible node S gets infected along SI links at a rate p, leading to the emergence of infectious node I and an increased probability of infection. Meanwhile, infectious node I recovers at a recovery rate r to become node R, reducing the probability of infection.

The evolution equation for node R indicates that, on average, only the transitions from infectious node I and the state change of node R itself affect the evolution of node R. This is because infectious node I switches to recovery node R at a rate of r, increasing the probability of recovery. Meanwhile, recovery node R itself switches to susceptible node S at a rate of q, decreasing the probability of being in the recovery state.

Here one can get the evolution equation for links in this model. It is important to note that because mean-field quantities are used to establish the differential equations and the study focuses on the states of nodes and links, one must consider the interaction between these nodes and links. Otherwise, the system would not be closed. This interaction between nodes and links is reflected in all three terms in the network (see Fig. 1D).

For the evolution equation of SS-type links (Eq. 4), on average, only the evolution of SR and SI-type links, as well as the three-point motif SSI, affect the evolution of SS-type links. This is because recovered nodes R in SR links switch to susceptible nodes S at a rate of q, thereby increasing the probability of SS links. When susceptible nodes S form SI links with infected nodes, in order to avoid infection, S nodes disconnect from I nodes and rewire to S nodes at a rate of w (as illustrated in Fig. 1C(1), where $\frac{P_S}{P_S+P_R}$ represents the proportion of susceptible nodes among non-infected

nodes), thus increasing the probability of SS links. Additionally, considering the interactions between links and nodes, where K/N represents the average number of links around each node (average degree). As shown in Fig. 1D(1), when SS links form a three-point motif with neighboring I nodes, any S node in the SS pair gets infected at a rate of p, leading to a reduction in SS links.

In the link evolution Eq. 5 for the SI type, on average, only IR, SI links and ISI, SSI three-point motifs affect the evolution of SI links. In contrast to the third term in Eq. 4, when SS links form a three-node motif with neighboring I nodes resulting in a decrease in SS links and, consequently, an increase in SI links, the first term signifies the formation of SS links at a certain rate. In this process, any susceptible node S gets infected at a rate of p, leading to the formation of SI links (Fig. 1D(1)). The second term indicates that recovery nodes R within SR links revert to susceptible nodes S at a rate q, increasing the probability of SI links. The third term represents a recovery rate r for infectious node I within SI links to become a recovery node R, decreasing the probability of SI links. The fourth term indicates that susceptible node S, to avoid infection, has a rewiring probability w, reducing the probability of SI links. The fifth term signifies that susceptible node S gets infected at a rate p within SI links, decreasing the probability of SI links. The sixth term considers the interaction between SI links and neighboring I nodes, as illustrated in Fig. 1D(2). When SI links form a three-node motif ISI with neighboring I nodes, susceptible node S gets infected at a rate of p, reducing the probability of SI links. Simultaneously, this leads to an increase in the probability of II links, resulting in the second term in Eq. 6.

$$\dot{P}_S = qP_R - p\frac{K}{N}P_{SI} \tag{1}$$

$$\dot{P}_I = p\frac{K}{N}P_{SI} - rP_I \tag{2}$$

$$\dot{P}_R = rP_I - qP_R \tag{3}$$

$$\dot{P}_{SS} = qP_{SR} + w\frac{P_S}{P_S+P_R}P_{SI} - 2p\frac{K}{N}\frac{P_{SS}P_{SI}}{P_S} \tag{4}$$

$$\dot{P}_{SI} = 2p\frac{K}{N}\frac{P_{SS}P_{SI}}{P_S} + qP_{IR} - rP_{SI} - wP_{SI} - p\left(P_{SI} + \frac{K}{N}\frac{P_{SI}^2}{P_S}\right) \tag{5}$$

$$\dot{P}_{II} = p\left(P_{SI} + \frac{K}{N}\frac{P_{SI}^2}{P_S}\right) - 2rP_{II} \tag{6}$$

$$\begin{aligned}\dot{P}_{SR} = {} & rP_{SI} + w\frac{P_R}{P_S+P_R}P_{SI} + 2qP_{RR} - qP_{SR} \\ & - p\frac{K}{N}\frac{P_{SI}P_{SR}}{P_S} + w\frac{P_S}{P_S+P_R}P_{IR}\end{aligned} \tag{7}$$

$$\dot{P}_{IR} = 2rP_{II} + p\frac{K}{N}\frac{P_{SI}P_{SR}}{P_S} - qP_{IR} - rP_{IR} - wP_{IR} \tag{8}$$

$$\dot{P}_{RR} = rP_{IR} - 2qP_{RR} + w\frac{P_R}{P_S+P_R}P_{IR} \tag{9}$$

In the link evolution Eq. 6 of II, the first term considers infectious node S within SI links getting infected at a rate p, leading to the formation of II links. The third term considers infectious node I within II links with a recovery rate r, becoming recovery nodes R, decreasing the probability of II links.

In the link evolution Eq. 7 of SR, the first term indicates that infectious nodes I within SI links have a recovery rate r, switching to recovery nodes R, increasing the probability of SR links. The second term represents that susceptible nodes S within SI links, to avoid infection, disconnect and rewire to recovery nodes R at a rate w (as illustrated in Fig. 1C(1), where $\frac{P_R}{P_S+P_R}$ represents the proportion of recovery nodes among non-infected nodes), increasing the probability of SR links. The third term signifies that two recovery nodes R within RR links switch to susceptible nodes S at a rate q, increasing the probability of SR links. The fourth term indicates that recovery nodes R within SR links switch to susceptible infectious nodes S at a rate q, decreasing the probability of SR links. The fifth term considers the interaction between SR links and surrounding infectious nodes I, forming a three-node motif ISR (Fig. 1D (3)). In this motif, susceptible nodes S get infected at a rate of p, decreasing the probability of SR links and, conversely, increasing the probability of IR links (the second term in Eq. 8). The sixth term represents that recovery nodes R within IR links, to avoid infection, rewire to susceptible nodes S (as shown in Fig. 1C (2)), resulting in the formation of SR links and increasing their probability. ($\frac{P_S}{P_S+P_R}$ represents the proportion of susceptible nodes among non-infected nodes.)

In the link evolution Eq. 8 of IR, the first term represents II links with two infectious nodes I, having a recovery rate r, becoming recovery nodes R, increasing the probability of IR links. The second term considers SR links within a three-node motif ISR, where susceptible node S gets infected by infectious node I, increasing the probability of IR links (Fig. 1D (3)). The third term represents recovery nodes R within IR links with a rate q, becoming susceptible nodes I, decreasing the probability of IR links. The fourth term represents infectious node I within IR links with a recovery rate r, becoming recovery nodes R, decreasing the probability of IR links. The fifth term represents recovery nodes R within IR links, rewiring to avoid being infected by infectious nodes I, decreasing the probability of IR links (Fig. 1C (2)).

In the link evolution Eq. 9 of RR, the first term represents infectious node I within IR links with a recovery rate r, becoming a recovery node R, increasing the probability of RR links. The second term represents two recovery nodes R within RR links, with a rate q, becoming susceptible nodes S, decreasing the probability of RR links. The third term represents recovery nodes R within IR links, to avoid infection by infectious nodes I (as shown in Fig. 1C (2)), rewiring to become recovery nodes R, increasing the probability of RR links. ($\frac{P_R}{P_S+P_R}$ represents the proportion of recovery nodes among non-infected nodes.)

One of the key findings of this study is that the model exhibits bistable behavior compared to static networks without rewiring, indicating the presence of two stable states: disease-free equilibrium and epidemic equilibrium. This is compared to static network models without the introduction of rewiring (Fig. 1 (a) in research paper (46)), which typically give a single attractor state of endemic in a wide range of infection rates. However, after the introduction of rewiring, two stable states emerged obviously, the endemic state and the disease-free state. The main reason for the appearance of bistable states is the interplay between the dynamic rewiring characteristics and the topology of adaptive networks. The adaptive rewiring facilitates the isolation of infected individuals, significantly increasing the epidemic threshold. However, in doing so, the rewiring introduces a mixing of connections within the population, leading to the formation of a highly connected susceptible cluster characterized by a larger variance in the degree distribution, thus resulting in a lower

epidemic threshold. Consequently, the local effect of rewiring tends to suppress the epidemic, whereas the topological effect promotes its occurrence (45). This is because, with an increase in the rewiring rate, the network's topology changes, leading to the formation of highly non-infected clusters within the network, making it easier to promote the disease transmission. In this scenario, rewiring does not completely separate the infected from the non-infected, rather, it structures the network into two loosely connected clusters of non-infected and infected individuals. Although connections between clusters are continuously removed by rewiring, new links are generated by the transmission dynamics of nodes within these two clusters, namely susceptible, infected, and recovered (SIRS) dynamics. Thus, in the case of adaptive rewiring and epidemic dynamics, a dynamic equilibrium state emerges in the network, where both the structure of the network and the states of its nodes remain stable to a certain extent, and the number of connections within and between clusters, as well as the number or proportion of non-infected and infected individuals, remains constant, making bistability possible under appropriate rewiring rates.

In Fig. 1C(1), when a group of healthy or susceptible individuals becomes aware of an infected person around them, they adjust their behavior to avoid contact with the disease. For example, more frequent hand-washing, wearing a mask when infected, and self-isolation are all examples of adaptive behaviors in the presence of disease, and in networks represented by populations, rewiring largely reflects how people respond to the situation (56), so rewiring promotes isolation of infected individuals, the effect of which tends to suppress the outbreak. This is compared to a stable local endemic state without the introduction of rewiring and the emergence of a new disease-free state (45).

The introduction of rewiring influences both the network structure and epidemic dynamics, resulting in a bistable region with coexisting endemic and disease-free states. A distinct bistable state is observed within a certain range of infection rate values p this bistable behavior offers a new perspective for understanding the dynamic processes of epidemics, emphasizing the complexity and diversity of dynamic adaptive networks in epidemiology (45, 63). From a non-equilibrium perspective, the study also explores the behavior of power-law scaling in fluctuations near bifurcation points. While revealing the bistable behavior, researchers also highlighted the challenges one faces in modeling epidemic transmission behavior in dynamic networks. However, in non-equilibrium processes, the physical mechanisms behind the dual stability of disease-free and endemic states remain not fully elucidated. There is still a lack of comprehensive understanding of the deeper dynamics and thermodynamic mechanisms involved in these non-equilibrium processes.

Methods

Landscape and flux theory

Since Isaac Newton formulated the Newtonian equation for dynamics $m\ddot{\boldsymbol{x}} = \boldsymbol{F}$, there has been a keen interest in solving differential equations. Once the initial conditions of the equation are known, the dynamics of the system at any future time are determined. Typically, deterministic equations $\dot{\boldsymbol{x}} = \boldsymbol{F}(\boldsymbol{x})$ are employed for studying the complex nonlinear dynamics of a network. In this context, the meaning of $\boldsymbol{F}$ varies depending on the specific research subject. For instance, in the context of chemical reactions where $\boldsymbol{x}$ represents a concentration vector and $\boldsymbol{F}(\boldsymbol{x})$ is the vector of reaction rate flows, this equation can be regarded as a degenerate form of Newton's equations under overdamping conditions.

While deterministic equations offer detailed insights into the system's evolution, their descriptions are often implicit in many cases. The dynamics of a system are inevitably influenced by both internal and external factors, typically in a non-negligible manner (64–68). Taking this effect into account, the general network dynamics should be a stochastic process, and researchers commonly use Langevin equations describing Brownian motion to characterize the dynamical process (58, 59, 66, 68), i.e. $\dot{\boldsymbol{x}} = \boldsymbol{F}(\boldsymbol{x}) + \boldsymbol{\eta}$, where $\boldsymbol{F}(\boldsymbol{x})$ represents the deterministic driving force, $\boldsymbol{\eta}$ is the noise with a Gaussian distribution satisfying the autocorrelation function $\langle \boldsymbol{\eta}(\boldsymbol{x}, \boldsymbol{t})\boldsymbol{\eta}(\boldsymbol{x}, \boldsymbol{0})\rangle = \boldsymbol{D}\boldsymbol{\delta}(\boldsymbol{t})$, and $\boldsymbol{D}$ is the diffusion coefficient, reflecting the magnitude and uniformity of fluctuations. The diffusion coefficient can be defined as the strength of the autocorrelation function of the stochastic force at different times, and thus representing the strength of the noise or fluctuations. In general, the diffusion coefficient is a tensor or matrix. However, in our study, only isotropic and homogeneous Gaussian white noise is considered, and it is set as a constant.

Building upon this foundation, we shift our focus from deterministic trajectories to the statistical behavior of these trajectories. Through long-term stochastic dynamic simulations, we obtain the steady-state probability distribution of the variable $\boldsymbol{x}$. The evolution of the probability distribution in the state space follows the Fokker–Planck equation (66, 69) $\nabla \cdot \boldsymbol{J} + \frac{\partial P}{\partial t} = 0$, where P is probability function. At steady state, by defining $U = lnPss$, we can derive the non-equilibrium potential function U, which is similar to the Boltzmann distribution in an equilibrium system. Once we ascertain the steady-state probability distribution and the non-equilibrium potential function, we can derive the thermodynamic characteristics, stability, robustness, and more for the entire infectious disease network or system. The flux is defined $\boldsymbol{J} = \boldsymbol{F}P - \nabla \cdot \boldsymbol{D}P$. The divergence of the flux is zero at steady state. Furthermore, since the divergence of flux is zero $\nabla \cdot \boldsymbol{J_{ss}} = 0$, there are two possibilities: the first is flux being zero $\boldsymbol{J_{ss}} = 0$, indicating no net flux, and the system is in equilibrium satisfying detailed balance. The second is flux being non-zero and representable as a rotational field, indicating the system is in a non-equilibrium state violating detailed balance.

The overall driving force of the system can be decomposed into a gradient force and a rotational force: $\boldsymbol{F} = -\boldsymbol{D} \cdot \nabla U + \nabla \cdot \boldsymbol{D} + \frac{\boldsymbol{J_{ss}}}{P_{ss}}$ (58, 59, 70, 71). We know that when there is only an electric field, electrons move in a manner following the electric potential gradient (electric field). This describes the dynamics of an equilibrium system with detailed balance, while the net flux is zero. However, when the net flux is non-zero, the detailed balance is broken, and the system is in nonequilibrium. This is the case when the electric and magnetic fields act together, electrons undergo spiral motion under the combined effects of the electric and magnetic fields. The dynamical evolutions resulting from the decomposition of the driving force are very similar to the motion of charged particles under electric and magnetic fields (58–60).

Non-equilibrium thermodynamic mechanics

The rate of entropy production is closely related to dissipation (72). In statistical mechanics, entropy is defined as:

$$S = -\int P(\boldsymbol{x}, t) \ln P(\boldsymbol{x}, t) \boldsymbol{dx},$$

and the rate of change of entropy with respect to time can be obtained by taking the derivative with respect to time:

$$\dot{S} = \int (\boldsymbol{J} \cdot \boldsymbol{D^{-1}} \cdot \boldsymbol{J})/P \boldsymbol{dx} - \int (\boldsymbol{J} \cdot \boldsymbol{D^{-1}} \cdot (\boldsymbol{F} - \nabla \cdot \boldsymbol{D})) \boldsymbol{dx}$$

(40, 71, 72). The first term in the equation is defined as entropy production rate (EPR), and the second term is defined as thermal dissipation (HDR). In a steady state, the rate of entropy production equals the rate of thermal dissipation. Non-equilibrium systems are open systems that continuously exchange energy and information with the environment, among other factors. The unique properties of dissipative non-equilibrium systems are closely related to dissipation and entropy production rates in the steady state of non-equilibrium systems (73).

Flickering frequency

The average dynamical time required for the system to transition from one stable state to another reflects the difficulty of different state transitions. When the barrier height is relatively low, it is anticipated that the mean first-passage time (MFPT) from the epidemic state to the non-epidemic state will decrease, and correspondingly, its reciprocal frequency will sharply increase. This indicates that frequency can serve as a crucial indicator for impending warning signals. We term the frequency near the dynamical phase transition point as the flickering frequency, which has been shown to act as an early predictive indicator (61).

Time reversal symmetry breaking

Correlation functions can be utilized to assess the degree of detailed balance breakdown or the level of time irreversibility in a system (74–78). Here, we have computed the average difference between forward and backward cross-correlations, defined as:

$$\Delta CC = \sqrt{\frac{1}{t_f}\int_0^{t_f} \left(C_{XY}(\tau) - C_{YX}(\tau)\right)^2 \mathrm{d}\tau}$$

Here, $C_{XY}(\tau)$ represents the forward cross-correlation function in time, defined as:$C_{XY}(\tau) = \langle X(0)Y(\tau)\rangle = \sum X^i Y^j P_i^{ss} P_{ij}(\tau)$. $C_{YX}(\tau)$ is the backward cross-correlation function in time, where X and Y represent the time series of two random variables, and τ denotes the lag time between the two series. P_{ij} is the probability from state i to state j at time τ. The quantity ΔCC provides directional information about non-equilibrium flux (74). By analyzing the asymmetry of relevant functions, we can comprehend the dynamic characteristics of non-equilibrium networks and potentially make predictions about critical points. The breakdown of detailed balance in time dynamics is further evaluated through the computed measures of cross-correlation. As a system approaches a critical point, the increasing asymmetry in temporal correlations suggests a deviation from process reversibility. The broken of time-reversal symmetry corresponds to the net flux, thereby supporting the idea that the system is approaching a critical transition.

Critical slowing down

Physics provides a comprehensive perspective on the evolution of infectious disease models (21). For instance, traditional deterministic compartmental models of infectious diseases (32, 33), employing systems of ordinary differential equations, leverage techniques from nonlinear dynamical systems theory. Similarly, stochastic models of specific infectious diseases (35, 36) draw upon methods from statistical physics. In the field of statistical physics, critical slowing down is a conceptual framework that elucidates the prominent fluctuation behavior experienced by a system as it approaches the critical point for a continuous transition just before switching from one phase to another. These fluctuations manifest not only in an increased amplitude but also in prolonged durations of fluctuations, deceleration in the recovery rate from disturbances, and a diminished capability to revert to the previous phase (79, 80). The concept of critical slowing down holds paramount significance in statistical physics, as it aids in identifying specific indicators of a system approaching the critical transition point, thereby providing early warning signals for an impending phase transition (80). A comprehensive understanding of phase transition behaviors and the natures of systems in the vicinity of critical points is crucial for in-depth research.

Scheffer and colleagues, in their research, observed the occurrence of critical slowing down as a system gradually approaches a bifurcation point. This behavior gave rise to three potential precursor signals, namely, a deceleration in the recovery from disturbances, an increase in autocorrelation coefficients, and an augmentation of variance (81). The identification and analysis of these signals contribute to a more nuanced comprehension of the system's behavior near critical points, making it crucial for the study of phase transition behaviors and their occurrences (82–84).

Results and discussion

Landscape and flux in epidemic models under adaptive networks

Noise is a part of the complexity of biological systems and can exert effects across different biological scales. For instance, noise in biological gene expression may disrupt cellular signaling, circadian rhythms, and developmental processes (85, 86). Similarly, infectious diseases are unavoidably influenced by various stochastic factors during the course of their pathogenesis. For example, in studies of cholera, it has been found that significant noise interference may lead to disease extinction (35). Therefore, models considering the impact of stochastic factors on infectious diseases would be more practical. Previous studies have indicated that bistability can emerge in epidemic models of adaptive network rewiring (46). However, the thermodynamic and dynamic mechanisms underlying this bifurcation and the predictive methods remain challenging. Building upon the mean-field equations (46, 63), we developed a stochastic dynamical model incorporating isotropic Gaussian white noise. The diffusion coefficient, previously denoted by $\boldsymbol{D}$, is now represented by D and is a constant. We obtained the steady-state probability distribution function through stochastic dynamical simulations and subsequently derived the potential function U. Once the potential function was obtained, a deeper understanding of the network's global description and stability measure was achieved, including stable states, phase transitions, and other critical features. For visualization purposes, summation and averaging over other dimensions were performed to select two state variables, creating a representation of the network's potential landscape. In Fig. 2, three-dimensional visualizations of the landscape under different state variables are presented. The system's driving force can be decomposed into the potential landscape gradient and the corresponding rotational flux. The gradient force stabilizes the network at a stable attractor, while the rotational force drives the system away from the stable attractor.

In the practice, it is difficult to determine whether the infection rate of a specific disease is a constant or not, because the actual disease has to go through various stages in the process of transmission, from emergence and transmission to the

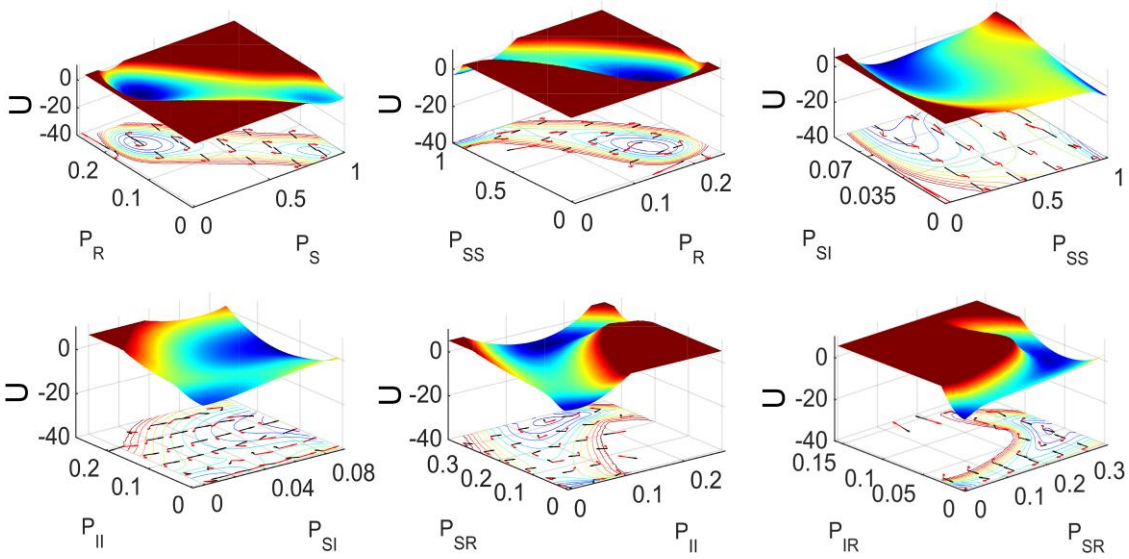

Fig. 2. Three-dimensional landscape projections were selected for different state variables, showing a three-dimensional landscape with two variables fixed in a bistable phase. The infection rate p is fixed at 1.58×10^{-3}, and the diffusion coefficient is $D = 1.7 \times 10^{-6}$. The coordinates of disease-free state are (1,0,0,1,0,0,0,0,0), while The coordinates of the endemic state are (0.18085, 0.62411, 0.19504, 0.26094, 0.07900 ,0.16748, 0.32534, 0.06021, 0.10703). Contour plots of the landscape are also shown at the bottom of the figure, where black arrows at the bottom represent gradient forces $-D\nabla U$, and red arrows represent rotational driving force flux $\frac{J_{SS}}{P_{SS}}$.

awareness by people of the changes. We believe that infection rate is generally not constant. For simplicity, one sets the infection rate as being constant for the simplification of modeling. Figure 3 displays the three-dimensional potential landscape U as a function of recovery node probability and susceptibility link probability, illustrating the global features of the infectious disease network. At very low infection rate, disease-free state dominates with a stable basin of attraction. Upon an increase in the infection rate, the stable endemic state emerges. As the infection rate continues to rise, the system switches from the disease-free state to the endemic state. Eventually, the endemic state becomes dominant, and the disease-free state disappears.

Thermodynamic and dynamical origins of non-equilibrium phase transitions

In this study, we developed non-equilibrium thermodynamics and applied it to an adaptive epidemic network. Non-equilibrium open systems continuously interact with the external environment, involving exchanges of energy, information, and matter, leading to dissipation (58, 59).

Rotational flux can serve as a non-equilibrium feature of interactions between the internal and external components of a system coupled to its environment (58–60, 70). The emergence of net flux disrupts the equilibrium state, and changes in the flux directly influence the topology of the entire landscape, thereby providing a dynamic source for non-equilibrium phase transitions or bifurcations (75, 87). As shown in Fig. 4, we calculated entropy production, thermal dissipation, and flux in a non-equilibrium adaptive epidemic network under different infection rates in a steady-state scenario. Evidently, the equivalence between the rates of entropy production and heat dissipation is noted. Our computational results further reveal a distinctive trend wherein both entropy production and thermal dissipation exhibit an initial increase followed by a subsequent decrease in response to the infection rate, culminating in their peak values at a juncture where p approximates 0.00155. At this point, the weights of the epidemic state and the disease-free state are nearly equal, corresponding to a first-order phase transition point.

As shown in Fig. 4B and Fig. 4C, the entropy production rate and heat dissipation rate reach their maximum values at this point, indicating that the system experiences maximal dissipation and the highest level of non-equilibrium. This also suggests the potential existence of other dynamical phase transition points (bifurcation points) on both sides of the thermodynamic phase transition point, precisely corresponding to the monostable spinodal transition points of disease-free and endemic, as illustrated in Fig. 4A.

As described above, under non-equilibrium conditions, we decompose the driving force into gradient force and rotational flux. Due to the rotational nature of flux, it usually renders the individual states unstable. Meanwhile, the entropy production rate reflects the degree of system thermodynamic dissipation and non-equilibrium nature. As illustrated in Fig. 4B, Fig. 4D, and Fig. 3, with an increase in the infection rate p, the flux initially remains small, resulting in a single stable disease-free state with relatively low dissipative and maintenance costs. Upon a further increase in the infection rate, the flux intensifies, diminishing the stability of the disease-free state, prompting the gradual emergence of the endemic state, establishing a bistable coexistence scenario characterized by maximum non-equilibrium and maximum dissipative costs. With a further increase in the infection rate, the flux between the two states decreases, reducing the stability of the bistable basins of disease-free and endemic states. Consequently, only a single stable endemic state is formed, accompanied by a corresponding decrease in dissipative and maintenance costs. This indicates that the flux serves as the dynamical source driving non-equilibrium phase transitions, while the entropy production rate provides the supply cost, serving as the thermodynamic source of non-equilibrium phase transitions.

Therefore, by observing variations in flux and EPR, we can comprehend the non-equilibrium nature and stability of the internal dynamics of the entire infectious disease network. This understanding elucidates how non-equilibrium dynamics propel the system through bifurcations, orchestrating transitions from a

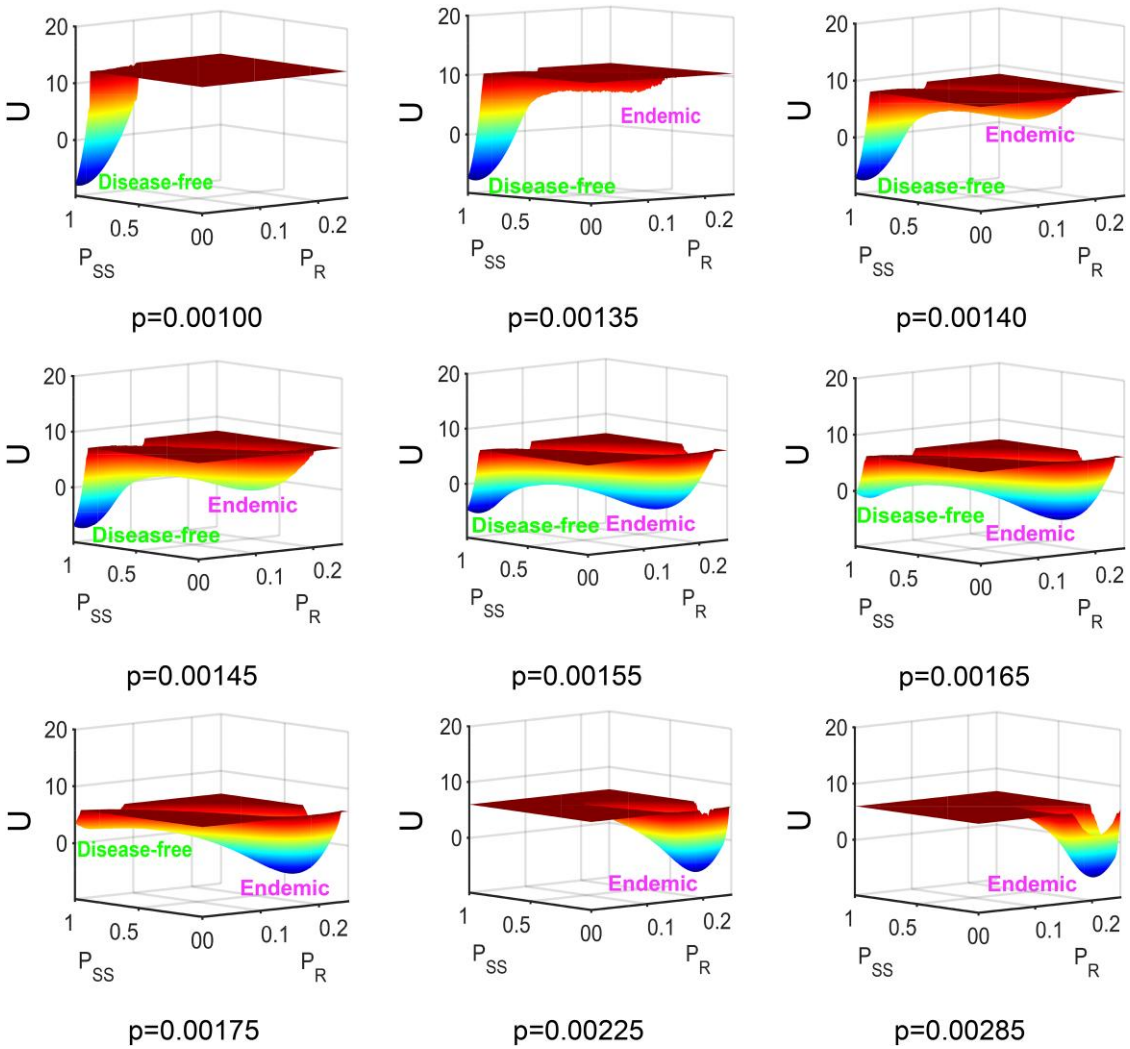

Fig. 3. Three-dimensional visual landscape projections on the recovery node recovery node and susceptibility link probability and susceptibility link probability under different infection rates p. The figures are annotated with attractors corresponding to the endemic state and the disease-free state, and specific values of different infection rates are provided at the bottom of each subplot. In all of these subplots, the diffusion coefficient is $D = 1.7 \times 10^{-6}$.

disease-free state to an endemic state. These insights contribute to understanding the intricate phase transitions inherent in complex systems such as infectious diseases, providing a broader perspective on the dynamic behavior and interactions within these intricate systems.

The advantage of EPR over lyapunov function potential is on the nonequilibrium. Since the flux provides the nonequilibrium driving force is rotational, it does not favor to localize in the specific place in state space. While the landscape gradient tends to attract the system to the stable basin, the flux being rotational tends to destabilize it. Thus increasing the flux can cause the instability or phase transition. For the saddle node bifurcation, near bifurcation, a stable basin of attraction can become flat , and thus the associated response or relaxation time becomes long. However, since EPR is directly related to the flux, it provides the thermodynamics origin of critical transitions. While flux or EPR can provide an warning signals earlier than that given by the landscape due to their cause for the instability.

Theoretically, flux and EPR can serve as early warning signals. For instance, in Fig. 3, different infection rates p correspond to distinct landscapes, along with their respective flux and EPR values. In practical terms, forecasting critical points involves monitoring the trends of flux and EPR as infection rates vary. For example, in the context of the saddle-node bifurcation examined in this study, both flux and EPR exhibit a peak with changes in the infection rate p shown in Fig. 4. This allows for the anticipatory identification that near this peak, bifurcation from bistable to monostable states emerges and the endemic state becomes dominant. Thus, in practice, observation of the trends in flux and EPR offers a feasible method for predicting critical points.

Barrier height and the mean first passage time

In epidemic models of adaptive SIS and SIRS networks, a rich dynamics can be observed (45, 46). However, traditional nonlinear dynamics mainly focus on local stability analysis near endemic or disease-free equilibrium points, overlooking the analysis of the dynamical processes themselves. Within the framework of landscape and flux theory, the local endemic and disease-free attractor basins are integrated, providing a global description of the dynamics. This global approach to dynamic description has been successfully applied in studying the overall properties and stability of complex systems. For instance, it has been used to quantify

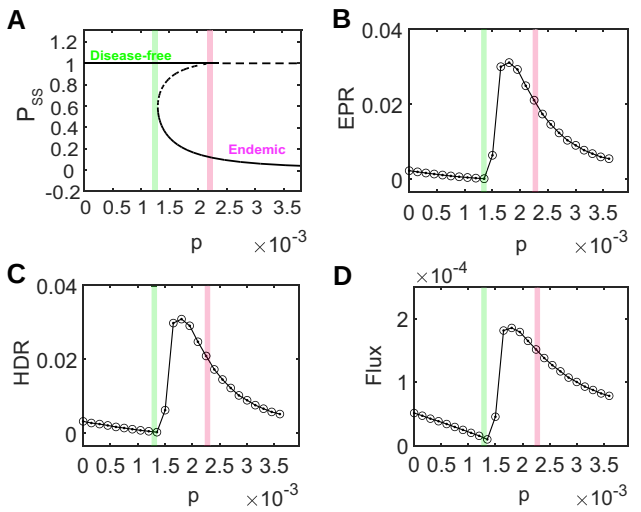

Fig. 4. A) The phase diagram versus parameter p, the solid lines in the figure represent stable solutions, while the dashed lines represent unstable solutions, with two bifurcation points occurring approximately at $p = 0.001298$ and $p = 0.002186$. B,C) The entropy production rate and the heat dissipation rate versus parameter p. D) The flux versus parameter p. The diffusion coefficient $D = 1.7 \times 10^{-6}$ used in the calculations.

the global stability, kinetic speed, and dominant paths of state switching in ecological systems (88), human brain sleep cycles (89), and the mechanisms of cancer tumor occurrence (90).

The landscape quantifies the global stability of the network, and the barrier height between potential basins reflects the difficulty of transitions between epidemic and disease-free states (58, 59). A higher barrier height indicates a more harder transition between the two states. We define the barrier height as the potential energy difference between the landscape saddle point and the landscape minimum: $\Delta U = U_{\text{saddle}} - U_{\text{min}}$. As the infection rate p increases, switching from the disease-free state to the endemic state, the barrier height of the disease-free state gradually decreases, as illustrated in Fig. 3 and Fig. 5A, rendering the disease-free state increasingly unstable. Correspondingly, the time required for the transition from the disease-free state to the endemic state (Fig. 5B) gradually decreases. Conversely, during the transition from the endemic state to the disease-free state with a decrease in the infection rate p, evident in both Fig. 3 and Fig. 5D, the barrier height of the endemic state decreases gradually, indicating a decrease in the stability of the endemic state. Consequently, the time required for the transition from the endemic state to the disease-free state (Fig. 5E) decreases. Additionally, as shown in Fig. 5C and Fig. 5F, we observe an almost linear relationship between the barrier height and the logarithm of the mean first passage time. This observation suggests that higher barrier heights contribute to a more stable coexistence of the disease-free and endemic steady states, making the transition between them more difficult with increased passage time ($T_{MFPT} \sim e^{\Delta U}$ is approximately valid).

The above results demonstrate that as the infection rate p increases, the stability of the endemic attractor state increases, while the stability of the disease attractor state decreases. This explains why increasing the infection rate promotes the spread of the disease. Therefore, it is crucial for individuals to take corresponding measures to reduce the infection rate in daily life, emphasizing personal protection and so forth (91, 92).

Early warning in non-equilibrium dynamics

Predicting future risks of infectious diseases is an interdisciplinary endeavor, requiring collaborative efforts from epidemiologists, biologists, demographers, statisticians, computer scientists, and other experts (93). Timely prediction of disease outbreaks and understanding the dynamics of disease spread are crucial for formulating effective control and mitigation strategies. Over the years, various methods and models have been developed to forecast the spread of infectious diseases. These include classical compartmental modeling approaches (94), bibliometric methods (95), machine learning method (96), and deep learning models combined with big data analysis (97). Researchers can consider the pros and cons of the above methods to choose the appropriate approach for predicting disease trends. However, predictive methods for infectious disease dynamics modeled by nonlinear ODEs still pose challenges. Here, we employ three measures:flickering frequencies, critical slowing down, and time irreversibility to forecast bifurcation in a nonlinear dynamics-based infectious disease dynamical system.

We conducted calculations for the flickering frequency, critical slowing down, and cross-correlation describing time-reversal symmetry breaking, aiming to test the predictive capability of our theoretical framework for critical points. Readers can find more technical details in the supplementary material and all computations are available on https://github.com/lq1235/Infectious-disease. In Fig. 6, we present the computed results for these three physical quantities, serving as early warning signals that effectively anticipate the arrival of a critical point. These analytical findings robustly support our theory, emphasizing the changing trends of these physical quantities as the system approaches a critical state. This underscores their significance for further research and practical applications, providing crucial guidance for in-depth investigations.

To begin with, let us discuss starting from the disease-free state. From Fig. 6A–6C, it can be observed that as the infection rate increases and approaches the vicinity of the endemic state transition point, the flickering frequency, critical slowing-down relaxation time τ, and ΔCC exhibit noticeable increments. This indicates that these three parameters could serve as precursory signals for the onset of disease-free and endemic states. When the infection rate parameter p changes, the landscape's barrier height determines the difficulty of state transitions, thus determining the flickering frequency. It is understandable that, with variations in the control parameter p, when the barrier height is low around the transition point, the frequency sharply rises. In Fig. 3, it is evident that approaching the transition point, the disease-free state exhibits an increasingly flattened trend. This alteration results from the heightened elasticity of the disease-free state, indicating a slowing recovery rate. Correspondingly, from Fig. 6D–6F, assuming the state initially resides in an endemic state, as the infection rate diminishes toward the proximity of the transition point ($p = 0.00135$), the endemic state gradually flattens, resulting in a significantly increased relaxation time τ due to the slower recovery rate. Hence, critical slowing-down offers early predictions for infectious disease outbreaks and disappearances.

The crosscorrelation functions are closely associated with symmetry when describing the dynamical aspects of a system. In reversible equilibrium dynamics, crosscorrelation functions demonstrate symmetry, reflecting the system's time reversibility. However, in irreversible equilibrium dynamics, symmetry is broken, signifying the system's temporal irreversibility. This broken symmetry in dynamical systems likely mirrors the time

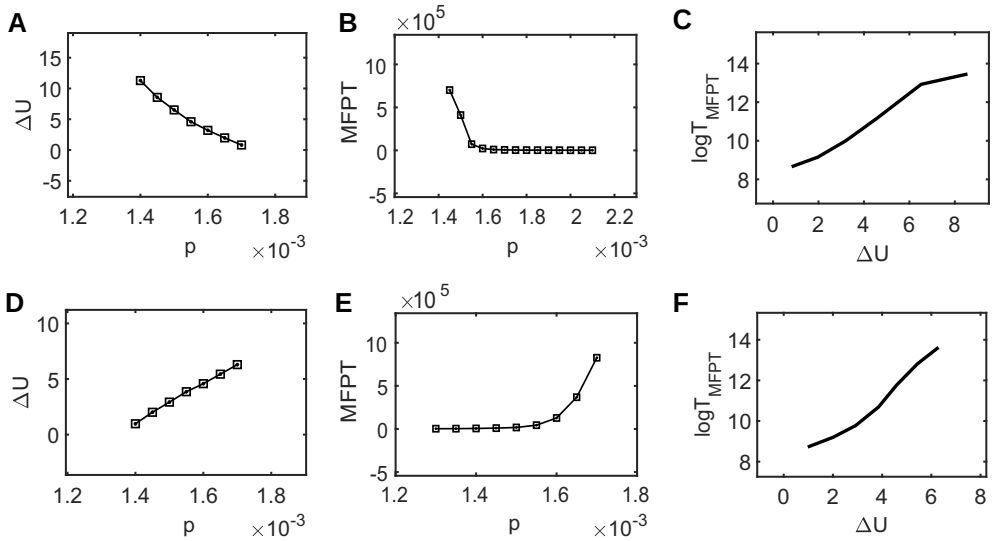

Fig. 5. A,D) Barrier height versus infection rate p. The barrier height refers to the energy barrier between two states (disease-free phase and endemic phase), specifically defined as the vertical distance or energy difference between the saddle point and the lowest points of potential energy U in the two states. B,E) Mean first passage time versus infection rate p. C,F) The logarithm of the mean first passage time in relation to the barrier height. MFPT specifically represents the average time taken to pass from the disease phase to the lowest point U in the disease-free phase. A–C) The results of calculations with the disease-free phase, meaning the initial conditions for solving the stochastic ordinary differential equation are chosen in this state. D–F) The results of calculations with the endemic phase. In all calculations, the diffusion coefficient D is set to 1.7×10^{-6}.

irreversibility of the system, implying a directional and irreversible characteristic in the system's evolution. This irreversibility, linked to phase transitions, serves as a dynamical source for these transitions. Notably, as illustrated in Fig. 6C, Fig. 6F, and Fig. 4D, the abrupt change in the average difference of crosscorrelation functions forward and backward in time near the critical point corresponds to the variation in system flux. This suggests that flux changes can be captured through alterations in time irreversibility of the crosscorrelation functions, offering insights into dynamical phase transitions, early warnings, and alterations in steady-state landscapes. Therefore, the symmetry or breaking thereof in correlation functions not only reflects the dynamical nature of a system but also serves as a means to interpret causal relationships in system state changes, providing a predictive tool for system phase transitions.

In Fig. 7, we conducted a comparative analysis of three proposed indicators for predicting critical points. It is noteworthy that our metric, the average difference of cross-correlation between functions forward and backward, often predicts the arrival of the critical point earlier than critical slowing down. This is attributed to the former being influenced by the change in flux, while the latter is induced by the critical deceleration as the system approaches the critical point. Our research suggests that, in general, the cross-correlation approach associated with the time irreversibility of non-equilibrium systems can often provide more effective warning signals than critical slowing down, while the flickering frequency serves as a later predictive indicator.

In practical applications, certain physical quantities like entropy production rate, flux, and heat dissipation rate are often difficult to directly observe or extract in experiments. However, we can readily access time series data of system state variables, which offer insights into irreversibility, flickering frequency, and critical slowing down phenomena. These time series data serve as a more feasible avenue for experimental observation and validation of our prediction methods, accounting for specific measurement sequences and experimental errors. The validation process is intricately linked to the problem domain under study, spanning fields such as ecology, evolution, and climate science. Our ongoing efforts focus on empirically applying our theoretical framework within these domains. In practice, it is more feasible to directly observe the evolutionary time series of state variables within disease network systems. By monitoring these variables, including measures like critical slowing down from autocorrelation functions, flickering frequency from counting the state switching, and time irreversibility from the crosscorrelation functions of the observables in the time series, we can better predict disease dynamics. This approach ensures that our predictions are grounded in observable time series and applicable to real-world scenarios.

Optimal path of non-equilibrium dynamics

The transmission and emergence of infectious diseases constitute a non-equilibrium process, where the transition pathways between endemic and disease-free states in the presence of driving forces are irreversible. According to the variational principle, the optimal main path should satisfy the condition that the action reaches an extremum, i.e. $\delta S = 0$. In Fig. 8A, we quantified the minimum action in length space, obtaining the optimal path (71, 98).

$$S_{HJ} = \int_{x_i}^{x_f} \sqrt{\frac{E_{\text{eff}} + V(\boldsymbol{x})}{D}} - \frac{1}{2D} F_l dl.$$

Here, E_{eff} is the effective Hamiltonian. $V(\boldsymbol{x})$ is potential. D is an isotropic diffusion coefficient. F_l represents the force function. In the context of detailed balance, F_l manifests as a purely gradient force. However, deviations from detailed balance introduce a rotational component to this force. Considering the effect of rotational forces, we observe that the dynamical path between the disease-free attractor and the endemic attractor is no longer a gradient path, nor is it a path passing through a landscape saddle point. Instead, when neglecting rotational forces, we find that the dynamical path between the disease-free attractor and the endemic attractor is reversible, in stark contrast to the irreversible paths in the presence of non-equilibrium rotational forces.

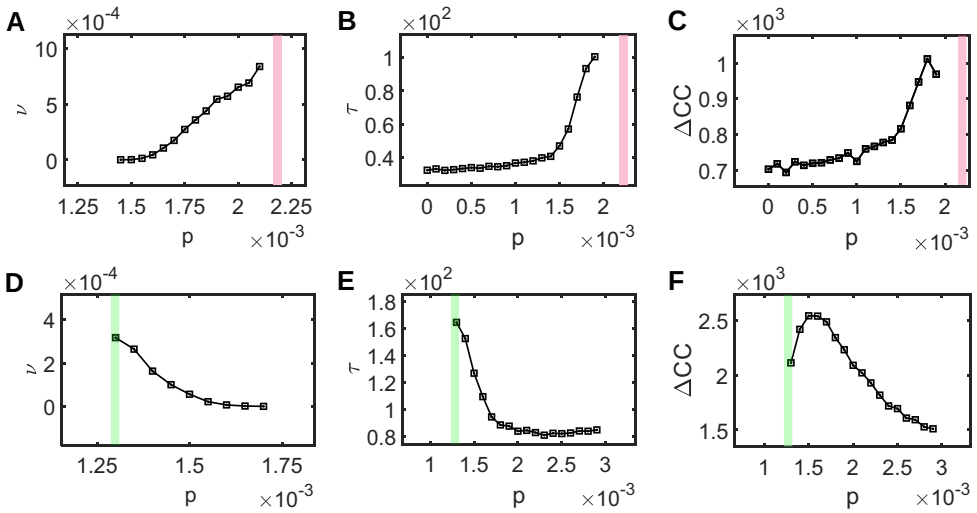

Fig. 6. A,D) Relationship between the flickering frequency ν and the infection rate p. B,E) Relationship between the autocorrelation relaxation time τ and the infection rate p. C,F) Relationship between the average difference in cross-correlation functions between time forward and time backward and the infection rate p. A–C) Computational results with the disease-free state as the initial point, while D–F) present the computational results with the endemic state as the initial point, where the diffusion coefficient is $D = 1.7 \times 10^{-6}$. The disease-free monostable and the endemic monostable are respectively at $p = 0.001298$ and $p = 0.002186$.

In non-equilibrium infectious disease networks, the impact of driving forces is influenced not only by the gradient of the potential landscape but also by non-equilibrium rotational forces. This results in the description of the dynamical process of non-equilibrium infectious disease networks as a spiral motion, distinct from the equilibrium state. Therefore, the presence of non-equilibrium rotational forces disrupts the gradient rule of dynamical paths, leading the paths to deviate from simple steepest descent trajectories. Instead, dynamical paths exhibit a spiral motion along the gradient direction, demonstrating unconventional dynamical characteristics in non-equilibrium systems. In the absence of rotational forces, reversibility of paths is preserved, however, once non-equilibrium rotational forces are considered, the dynamical paths of the system become irreversible, in stark contrast to the situation when rotational forces are ignored. The introduction of non-equilibrium rotational forces results in a richer and more complex dynamical behavior in the system.

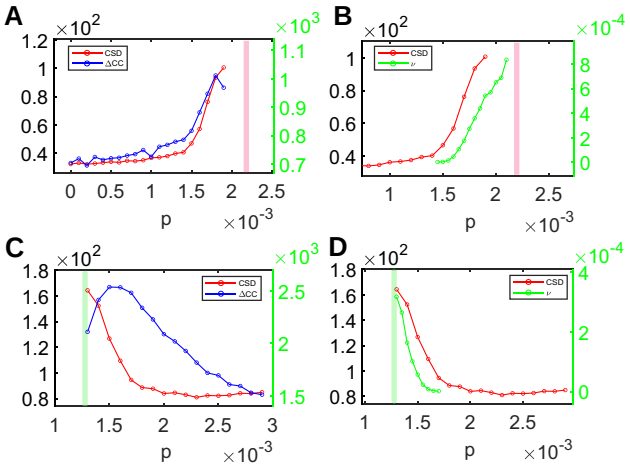

Fig. 7. A comparison of the early warning signs in Fig. 6. A,B) With disease-free as the calculation result of the initial state. C,D) With endemic as the calculation result of the initial state. In all subgraphs, critical slowing-down relaxation time (CSD) is referenced on the left y-axis. The average difference between forward and backward cross-correlations in Fig. 7A and Fig. 7C takes the right y axis as the reference. The flickering frequency in Fig. 7B and Fig. 7D takes the right y axis as reference.

Global sensitivity analysis

Various environmental factors play a crucial role in virus transmission (91). For instance, measures such as maintaining social distancing during pandemics (99) and disinfecting public areas can significantly reduce transmission rates, thereby curbing the spread of the virus. In adaptive networks, these individual protective behaviors are reflected in the dynamic rewiring of the network, particularly when non-infected individuals come into contact with infected ones, leading to network link rewiring (46).

To assess the relative importance of key parameters in an adaptive infectious disease network, we conducted a global sensitivity analysis on the barrier height. As mentioned earlier, the height of the barrier reflects the stability of different infectious disease states. If a state has a higher barrier, the system is less susceptible to external disturbances or less prone to state transitions. Figure 8B displays the variations in barrier height resulting from changes in different parameters. It is noteworthy that variations in the rewiring rate (w) lead to more significant changes in the barrier height for the disease-free state compared to the barrier height for the endemic state. This observation indicates that adjusting the parameter w is more likely to increase the barrier for the disease-free state, increasing its stability compared to the endemic state. Consequently, the system is more inclined to maintain a disease-free state and inhibit transitions to the endemic state. Therefore, a higher rewiring rate may be more effective in preventing infection and suppressing the spread of the disease. This is because rewiring implies that non-infected individuals (S, R) have less chance of contact with infected individuals (I) and maintain a certain level of isolation, thereby protecting themselves from infection. For example, the isolation of infected individuals (99–103) and the wearing of masks by individuals are manifestations of rewiring. Therefore, through the analysis of barrier height and its stability, we can easily understand why rewiring in infectious disease networks is more effective in

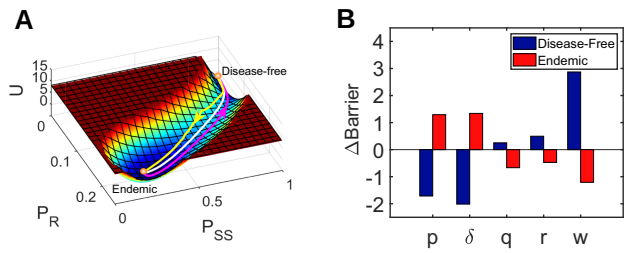

Fig. 8. A) Non-equilibrium dynamical paths. The line with an arrow represents the non-equilibrium optimal path between endemic and disease-free states in the presence of the rotational flux force, with the arrow pointing from the initial state to the final state. The line without an arrow represents the reversible path under equilibrium conditions. Here the infection rate is $p = 0.00158$, and $D = 1.7 \times 10^{-6}$. B) Global sensitivity analysis, the horizontal axis showcases the model's control parameters, while the vertical axis represents changes in barrier height. Using an infection rate of $p = 0.00155$ as a reference in the landscape, the chart depicts how the barrier heights for disease-free and endemic states change after a 5% increase for each parameter. Here the notation $\delta = K/N$ indicates how many links there are on average per node in the epidemic network.

promoting the emergence of the disease-free state while preventing the spread and diffusion of the disease.

Furthermore, our observations reveal a significant impact of the infection rate p and the average node degree $\delta = K/N$ on the barrier height. Our computational analyses demonstrate that increasing the infection rate p is more adept at decreasing the barrier height for the disease-free state, while concurrently exhibiting a heightened effect on increasing the barrier height for the endemic state. Simultaneously, an increase in the average number of links(δ) surrounding each node results in a decrease of the barrier height for the disease-free state and an increase of the barrier height for the endemic state. Similar to the previous analysis on rewiring, we see that higher infection rates p and a greater number of links surrounding each node ($\delta = K/N$) increase the stability of the endemic state while concurrently decrease the stability of the disease-free state. Conversely, lower infection rates p and a fewer number of links surrounding each node ($\delta = K/N$) decrease the stability of the endemic state while simultaneously increase the stability of the disease-free state. This observation aligns seamlessly with our empirical understanding, as higher infection rates accelerate the spread of the disease within the population, thereby propelling the progression of an epidemic. Conversely, lower infection rates (92) inhibit the spread of the disease within the population, thereby thwarting an epidemic. Additionally, a higher number of links around nodes implies an increasing number of contacts around individuals (higher K/N), significantly elevating the risk of individuals contracting the disease. In contrast, a lower number of links around each node implies fewer contacts among individuals (lower K/N), thereby reducing the risk of disease spread. This is consistent with the preventive measures outlined in the literature (55). Therefore, we should take measures such as vaccination or other relevant interventions to reduce the rate of infection of the disease (p) and minimize individual clusters (δ or w) in order to curb the spread and spread of the epidemic.

Conclusion

In this study, we employ the framework of landscape and flux theory in non-equilibrium statistical physics to investigate the stochastic dynamics based on an adaptive SIRS network. This approach allows for a quantitative and comprehensive elucidation of the underlying physical processes governing the non-equilibrium dynamics of infectious diseases. We provide a theoretical analysis of thermodynamics and dynamics for the prediction of epidemics. Such analyses are generally absent in typical deterministic compartmental epidemic models, such as the SIS models (45) and SIR models (104, 105), based on ordinary differential equations.

The spread of infectious diseases is described as two basins of attraction, and the dynamics of the infectious disease network system are determined by both gradient force and rotational flux force. Entropy production provides thermodynamic sources for supporting the infectious disease network, while flux provides dynamical sources.

In addition, our study also indicates that critical slowing-down, time irreversibility, and flickering frequency can serve as early warning indicators for predicting critical transitions, with time irreversibility being more easily observed directly from experiments compared to entropy production and flux. The presence of rotational flux as a non-equilibrium driving force results in an irreversible dominant pathway between infectious disease states.

Global sensitivity analysis of barrier height reveals that during epidemic spread, behaviors such as isolating from infected individuals, maintaining social distancing (w), or taking measures to reduce the infection rate (p) and minimize individual gatherings (lowering δ) all play a crucial role in curtailing the transmission of epidemics (55, 91, 92).

In summary, our simulation results are based on the adaptive SIRS model with the empirical parameters estimated from the previous studies (46). Using the actual experimental data, the model can be calibrated and validated to further improve the prediction accuracy and practicability of the model. Combining with experimental observations can bring the model closer to reality, thereby enhancing its ability to predict and manage disease outbreaks, and we are working on this. Our study reveal the dynamics of infectious disease spread and prediction from a non-equilibrium perspective, providing valuable insights into the complex nature of infectious diseases. Our study also provides a quantitative and physical description of the dynamics of infectious diseases and offers a practical approach for predicting critical transitions (bifurcation or non-equilibrium phase transition) of infectious disease. The proposed landscape and flux theoretical framework is generally applicable and can be extended to diverse fields such as medicine and biology.

Acknowledgments

The authors thank the useful discussions with colleague Han Yan, and the reviewers for their valuable suggestions.

Supplementary Material

Supplementary material is available at *PNAS Nexus* online.

Funding

This work is supported by funds from the National Natural Science Foundation of China (Grant No. 21721003 and No. 12234019).

Author Contributions

L.Q.W. data curation, investigation, visualization, writing-original draft, writing-review and editing. K.Z. resources, methodology. L.X. resources, investigation. J.W. conceptualization, resources, software, formal analysis, supervision, funding acquisition,

investigation, methodology, writing-original draft, project administration, writing-review and editing.

Data Availability

All the data and simulation source code used in this study is publicly available on Github. https://github.com/lq1235/Infectious-disease.

References

1 Moreno Y, Pastor-Satorras R, Vespignani A. 2002. Epidemic outbreaks in complex heterogeneous networks. *Eur Phys J B-Condens Matter Complex Syst*. 26:521–529.
2 Morens DM, Folkers GK, Fauci AS. 2004. The challenge of emerging and re-emerging infectious diseases. *Nature*. 430(6996):242–249.
3 Heesterbeek H, *et al*. 2015. Modeling infectious disease dynamics in the complex landscape of global health. *Science*. 347(6227):aaa4339.
4 COVID IHME Team Forecasting. 2021. Modeling covid-19 scenarios for the United States. *Nat Med*. 27(1):94–105.
5 Martin-Moreno JM, *et al*. 2022. Predictive models for forecasting public health scenarios: practical experiences applied during the first wave of the covid-19 pandemic. *Int J Environ Res Public Health*. 19(9):5546.
6 Tan Z-J, Zou X-W, Jin Z-Z. 2000. Percolation with long-range correlations for epidemic spreading. *Phys Rev E*. 62(6):8409.
7 Tan Z-J, Long C, Zou X-W, Zhang W, Jin Z-Z. 2002. Epidemic spreading in percolation worlds. *Phys Lett A*. 300(2–3):317–323.
8 Kuperman M, Abramson G. 2001. Small world effect in an epidemiological model. *Phys Rev Lett*. 86(13):2909.
9 Eubank S, *et al*. 2004. Modelling disease outbreaks in realistic urban social networks. *Nature*. 429(6988):180–184.
10 Piccardi C, Casagrandi R. 2008. Inefficient epidemic spreading in scale-free networks. *Phys Rev E*. 77(2):026113.
11 Campos PRA, Gordo I. 2006. Pathogen genetic variation in small-world host contact structures. *J Stat Mech Theory Exp*. 2006(12):L12003.
12 Gordo I, Campos PRA. 2007. Patterns of genetic variation in populations of infectious agents. *BMC Evol Biol*. 7:1–11.
13 Anderson RM, May RM. 1982. Directly transmitted infections diseases: control by vaccination. *Science*. 215(4536):1053–1060.
14 Grabowski A, Kosiński RA. 2004. Epidemic spreading in a hierarchical social network. *Phys Rev E*. 70(3):031908.
15 Saumell-Mendiola A, Serrano M, Boguná M. 2012. Epidemic spreading on interconnected networks. *Phys Rev E*. 86(2):026106.
16 Pastor-Satorras R, Castellano C, Van Mieghem P, Vespignani A. 2015. Epidemic processes in complex networks. *Rev Mod Phys*. 87(3):925.
17 Chang S, *et al*. 2021. Mobility network models of covid-19 explain inequities and inform reopening. *Nature*. 589(7840):82–87.
18 Pastor-Satorras R, Vespignani A. 2001. Epidemic spreading in scale-free networks. *Phys Rev Lett*. 86(14):3200.
19 Keeling MJ, Eames KTD. 2005. Networks and epidemic models. *J R Soc Interface*. 2(4):295–307.
20 Newman MEJ. 2003. The structure and function of complex networks. *SIAM Rev*. 45(2):167–256.
21 Brabers JHVJ. 2023. The spread of infectious diseases from a physics perspective. *Biol Methods Protocol*. 8(1):bpad010.
22 Logak E, Passat I. 2016. An epidemic model with nonlocal diffusion on networks. *Networks Heterogen Media*. 11(4):693–719.
23 Anderson RM, May RM. 1991. *Infectious diseases of humans: dynamics and control*. New York (NY): Oxford University Press.
24 Pastor-Satorras R, Vespignani A. 2002. Immunization of complex networks. *Phys Rev E*. 65(3):036104.
25 Cohen R, Havlin S, Ben-Avraham D. 2003. Efficient immunization strategies for computer networks and populations. *Phys Rev Lett*. 91(24):247901.
26 Bernoulli D, Blower S. 2004. An attempt at a new analysis of the mortality caused by smallpox and of the advantages of inoculation to prevent it. *Rev Med Virol*. 14(5):275.
27 Ross R. 1911. *The prevention of Malaria*. Vol. 6. London: John Murray.
28 Kermack WO, McKendrick AG. 1927. A contribution to the mathematical theory of epidemics. *Proc R S Lond Ser A Math Phys Charact*. 115(772):700–721.
29 Newman M. 2010. *Networks: an introduction*. New York (NY): Oxford University Press.
30 Beretta E, Takeuchi Y. 1995. Global stability of an sir epidemic model with time delays. *J Math Biol*. 33(3):250–260.
31 Cooke KL, Van Den Driessche P. 1996. Analysis of an seirs epidemic model with two delays. *J Math Biol*. 35:240–260.
32 Cooke K, Van den Driessche P, Zou X. 1999. Interaction of maturation delay and nonlinear birth in population and epidemic models. *J Math Biol*. 39:332–352.
33 Chowell G, Hengartner NW, Castillo-Chavez C, Fenimore PW, Hyman JM. 2004. The basic reproductive number of Ebola and the effects of public health measures: the cases of congo and Uganda. *J Theor Biol*. 229(1):119–126.
34 Rivers CM, Lofgren ET, Marathe M, Eubank S, Lewis BL. 2014. Modeling the impact of interventions on an epidemic of Ebola in Sierra Leone and Liberia. *PLoS Curr*. 6. https://doi.org/10.1371/currents.outbreaks.fd38dd85078565450b0be3fcd78f5ccf
35 Zhou X, Shi X, Wei M. 2022. Dynamical behavior and optimal control of a stochastic mathematical model for cholera. *Chaos, Solitons Fractals*. 156:111854.
36 Cai Y, Kang Y, Banerjee M, Wang W. 2015. A stochastic sirs epidemic model with infectious force under intervention strategies. *J Differ Equ*. 259(12):7463–7502.
37 Hyman JM, LaForce T. 2003. Modeling the spread of influenza among cities. In: Bioterrorism: mathematical modeling applications in homeland security. SIAM. p. 211–236.
38 Xue L, Scott HM, Cohnstaedt LW, Scoglio C. 2012. A network-based meta-population approach to model rift valley fever epidemics. *J Theor Biol*. 306:129–144.
39 Li MY. 2018. *An introduction to mathematical modeling of infectious diseases*. Vol. 2. Cham: Springer.
40 Wu Y, Sun Y, Lin M. 2022. Sqeir: an epidemic virus spread analysis and prediction model. *Comput Electr Eng*. 102:108230.
41 Roberts M, Andreasen V, Lloyd A, Pellis L. 2015. Nine challenges for deterministic epidemic models. *Epidemics*. 10:49–53.
42 van Kleef E, Robotham JV, Jit M, Deeny SR, Edmunds WJ. 2013. Modelling the transmission of healthcare associated infections: a systematic review. *BMC Infect Dis*. 13:1–13.
43 López-García M, Kypraios T. 2018. A unified stochastic modelling framework for the spread of nosocomial infections. *J R Soc Interface*. 15(143):20180060.
44 Fefferman NH, Ng KL. 2007. How disease models in static networks can fail to approximate disease in dynamic networks. *Phys Rev E*. 76(3):031919.
45 Gross T, D'Lima CJD, Blasius B. 2006. Epidemic dynamics on an adaptive network. *Phys Rev Lett*. 96(20):208701.
46 Shaw LB, Schwartz IB. 2008. Fluctuating epidemics on adaptive networks. *Phys Rev E*. 77:066101.

47 Bjørnstad ON, Finkenstädt BF, Grenfell BT. 2002. Dynamics of measles epidemics: estimating scaling of transmission rates using a time series sir model. *Ecol Monogr*. 72(2):169–184.
48 Garrett L. 2014. *Ebola: story of an outbreak*. UK: Hachette.
49 Ahituv A, Hotz VJ, Philipson T. 1996. The responsiveness of the demand for condoms to the local prevalence of aids. *J Human Res*. 31(4):869–897.
50 Philipson T. 1996. Private vaccination and public health: an empirical examination for us measles. *J Human Res*. 31(3):611–630.
51 Funk S, Salathé M, Jansen VAA. 2010. Modelling the influence of human behaviour on the spread of infectious diseases: a review. *J R Soc Interface*. 7(50):1247–1256.
52 Bornholdt S, Rohlf T. 2000. Topological evolution of dynamical networks: global criticality from local dynamics. *Phys Rev Lett*. 84(26):6114.
53 Holme P, Ghoshal G. 2006. Dynamics of networking agents competing for high centrality and low degree. *Phys Rev Lett*. 96(9): 098701.
54 Gross T, Blasius B. 2008. Adaptive coevolutionary networks: a review. *J R Soc Interface*. 5(20):259–271.
55 Wimalawansa SJ. 2020. Global epidemic of coronavirus–covid-19: what can we do to minimize risks. *Eur J Biomed*. 7(3): 432–8.
56 Schwartz IB, Shaw LB. 2010. Rewiring for adaptation. *Physics*. 3(17). https://doi.org/10.1103/Physics.3.17
57 Wu Q, Fu X. 2016. Immunization and epidemic threshold of an sis model in complex networks. *Physica A*. 444:576–581.
58 Wang J. 2015. Landscape and flux theory of non-equilibrium dynamical systems with application to biology. *Adv Phys*. 64(1): 1–137.
59 Fang X, Kruse K, Lu T, Wang J. 2019. Nonequilibrium physics in biology. *Rev Mod Phys*. 91(4):045004.
60 Wang J. 2022. Perspectives on the landscape and flux theory for describing emergent behaviors of the biological systems. *J Biol Phys*. 48(1):1–36.
61 Wang R, *et al.* 2012. Flickering gives early warning signals of a critical transition to a eutrophic lake state. *Nature*. 492(7429): 419–422.
62 Keeling MJ, Rand DA, Morris AJ. 1997. Correlation models for childhood epidemics. *Proc R Soc Lond Ser B: Biol Sci*. 264(1385): 1149–1156.
63 Shaw LB, Schwartz IB. 2009. Noise induced dynamics in adaptive networks with applications to epidemiology. In: Gross T, Sayama H, editors. *Adaptive networks. Understanding complex systems*. Berlin: Springer. p. 209–227.
64 Swain PS, Elowitz MB, Siggia ED. 2002. Intrinsic and extrinsic contributions to stochasticity in gene expression. *Proc Natl Acad Sci USA*. 99(20):12795–12800.
65 Thattai M, Van Oudenaarden A. 2001. Intrinsic noise in gene regulatory networks. *Proc Natl Acad Sci USA*. 98(15):8614–8619.
66 Van Kampen NG. 1992. *Stochastic processes in physics and chemistry*. Amsterdam: Elsevier.
67 Blomberg C. 2006. Fluctuations for good and bad: the role of noise in living systems. *Phys Life Rev*. 3(3):133–161.
68 Hu G. 1995. *Stochastic force and nonlinear systems*. Shanghai: Shanghai Science Education.
69 Risken H. 1996. *Fokker-planck equation*. Berlin: Springer.
70 Wang J, Xu L, Wang E. 2008. Potential landscape and flux framework of nonequilibrium networks: robustness, dissipation, and coherence of biochemical oscillations. *Proc Natl Acad Sci USA*. 105(34):12271–12276.
71 Wang J, Zhang K, Xu L, Wang E. 2011. Quantifying the Waddington landscape and biological paths for development and differentiation. *Proc Natl Acad Sci USA*. 108(20):8257–8262.
72 Qian H. 2001. Mesoscopic nonequilibrium thermodynamics of single macromolecules and dynamic entropy-energy compensation. *Phys Rev E*. 65(1):016102.
73 Zhang K, Wang J. 2017. Landscape and flux theory of nonequilibrium open economy. *Physica A*. 482:189–208.
74 Qian H, Elson EL. 2004. Fluorescence correlation spectroscopy with high-order and dual-color correlation to probe nonequilibrium steady states. *Proc Natl Acad Sci USA*. 101(9):2828–2833.
75 Xu L, Wang J. 2020. Curl flux as a dynamical origin of the bifurcations/phase transitions of nonequilibrium systems: cell fate decision making. *J Phys Chem B*. 124(13):2549–2559. PMID: 32118436.
76 Zhang K, Wang J. 2018. Exploring the underlying mechanisms of the Xenopus laevis embryonic cell cycle. *J Phys Chem B*. 122(21): 5487–5499.
77 Li S, Liu Q, Wang E, Wang J. 2023. Quantifying nonequilibrium dynamics and thermodynamics of cell fate decision making in yeast under pheromone induction. *Biophys Rev*. 4(3):031401.
78 Liu Q, Wang J. 2020. Quantifying the flux as the driving force for nonequilibrium dynamics and thermodynamics in non-michaelis–menten enzyme kinetics. *Proc Natl Acad Sci USA*. 117(2):923–930.
79 Dakos V, *et al.* 2012. Methods for detecting early warnings of critical transitions in time series illustrated using simulated ecological data. *PLoS ONE*. 7(7):e41010.
80 Dakos V, *et al.* 2008. Slowing down as an early warning signal for abrupt climate change. *Proc Natl Acad Sci USA*. 105(38): 14308–14312.
81 Scheffer M, *et al.* 2009. Early-warning signals for critical transitions. *Nature*. 461(7260):53–59.
82 Yan H, Zhang F, Wang J. 2023. Thermodynamic and dynamical predictions for bifurcations and non-equilibrium phase transitions. *Commun Phys*. 6(1):110.
83 Xu L, Patterson D, Levin SA, Wang J. 2023. Non-equilibrium early-warning signals for critical transitions in ecological systems. *Proc Natl Acad Sci USA*. 120(5):e2218663120.
84 Wang L, Zhang K, Wang J. 2024. Early warning indicators of war and peace through the landscapes and flux quantifications. *Phys Rev E*. 109(3):034311.
85 Ozbudak EM, Thattai M, Kurtser I, Grossman AD, Van Oudenaarden A. 2002. Regulation of noise in the expression of a single gene. *Nat Genet*. 31(1):69–73.
86 Raser JM, O'Shea EK. 2004. Control of stochasticity in eukaryotic gene expression. *Science*. 304(5678):1811–1814.
87 Zhang K, Wang E, Wang J. 2021. Searching for the physical origin of bifurcations in non-equilibrium economy. *Eur Phys J B*. 94: 1–9.
88 Xu L, Patterson D, Staver AC, Levin SA, Wang J. 2021. Unifying deterministic and stochastic ecological dynamics via a landscape-flux approach. *Proc Natl Acad Sci USA*. 118(24): e2103779118.
89 Yan H, *et al.* 2013. Nonequilibrium landscape theory of neural networks. *Proc Natl Acad Sci USA*. 110(45):E4185–E4194.
90 Li W, Wang J. 2020. Uncovering the underlying mechanisms of cancer metabolism through the landscapes and probability flux quantifications. *IScience*. 23(4):101002.
91 Valsamatzi-Panagiotou A, Penchovsky R. 2022. Environmental factors influencing the transmission of the coronavirus 2019: a review. *Environ Chem Lett*. 20(3):1603–1610.

92 Li J-T. 2022. The impacts of reducing the infection rate and infection source on the transmission of emerging infectious diseases. *Discrete Dyn Nat Soc*. 2022:3473538.
93 Woolhouse M. 2011. How to make predictions about future infectious disease risks. *Philos Trans R Soc B Biol Sci*. 366(1573): 2045–2054.
94 Dimitrov NB, Meyers LA. 2010. Mathematical approaches to infectious disease prediction and control. In: Risk and optimization in an uncertain world. INFORMS. p. 1–25.
95 Yang W, Zhang J, Ma R. 2020. The prediction of infectious diseases: a bibliometric analysis. *Int J Environ Res Public Health*. 17(17):6218.
96 Kohli PS, Arora S. 2018. Application of machine learning in disease prediction. In: 2018 4th International Conference on Computing Communication and Automation (ICCCA). IEEE. p. 1–4.
97 Chae S, Kwon S, Lee D. 2018. Predicting infectious disease using deep learning and big data. *Int J Environ Res Public Health*. 15(8): 1596.
98 Wang J, Zhang K, Wang E. 2010. Kinetic paths, time scale, and underlying landscapes: a path integral framework to study global natures of nonequilibrium systems and networks. *J Chem Phys*. 133(12):125103.
99 Day T, Park A, Madras N, Gumel A, Wu J. 2006. When is quarantine a useful control strategy for emerging infectious diseases? *Am J Epidemiol*. 163(5):479–485.
100 Tang B, *et al*. 2020. The effectiveness of quarantine and isolation determine the trend of the covid-19 epidemics in the final phase of the current outbreak in China. *Int J Infect Dis*. 95:288–293.
101 Khan MMUR, Arefin MR, Tanimoto J. 2022. Investigating the trade-off between self-quarantine and forced quarantine provisions to control an epidemic: an evolutionary approach. *Appl Math Comput*. 432:127365.
102 Fraser C, Riley S, Anderson RM, Ferguson NM. 2004. Factors that make an infectious disease outbreak controllable. *Proc Natl Acad Sci USA*. 101(16):6146–6151.
103 Zhou D, Shi X, Zhou X. 2023. Dynamic analysis of a stochastic delayed seirs epidemic model with lévy jumps and the impact of public health education. *Axioms*. 12(6):560.
104 Muñoz-Fernández GA, Seoane JM, Seoane-Sepúlveda JB. 2021. A sir-type model describing the successive waves of covid-19. *Chaos, Solitons Fractals*. 144:110682.
105 Chen Y-C, Lu P-E, Chang C-S, Liu T-H. 2020. A time-dependent sir model for covid-19 with undetectable infected persons. *IEEE Trans Network Sci Eng*. 7(4):3279–3294.